ORIGINAL ARTICLE

Multiparametric PET/MR imaging biomarkers are associated with overall survival in patients with pancreatic cancer

Bang-Bin Chen[1] · Yu-Wen Tien[2] · Ming-Chu Chang[3] · Mei-Fang Cheng[4] · Yu-Ting Chang[3] · Shih-Hung Yang[5] ·
Chih-Horng Wu[1] · Ting-Chun Kuo[2] · I-Lun Shih[1] · Ruoh-Fang Yen[4] · Tiffany Ting-Fang Shih[1]

Abstract

Purpose To correlate the overall survival (OS) with the imaging biomarkers of dynamic contrast-enhanced magnetic resonance imaging (DCE-MRI), diffusion-weighted imaging (DWI), magnetic resonance spectroscopy, and glucose metabolic activity derived from integrated fluorine 18 fluorodeoxyglucose positron emission tomography (^{18}F–FDG PET)/MRI in patients with pancreatic cancer.

Methods This prospective study was approved by the institutional review board and informed consent was obtained from all participants. Sixty-three consecutive patients (mean age, 62.7 ± 12 y; men/women, 40/23) with pancreatic cancer underwent PET/MRI before treatment. The imaging biomarkers were comprised of DCE-MRI parameters (*peak, IAUC$_{60}$, K^{trans}, k$_{ep}$, v$_e$*), the minimum apparent diffusion coefficient (ADC$_{min}$), choline level, standardized uptake values, metabolic tumor volume, and total lesion glycolysis (TLG) of the tumors. The relationships between these imaging biomarkers with OS were evaluated with the Kaplan-Meier and Cox proportional hazard models.

Results Seventeen (27%) patients received curative surgery, with the median follow-up duration being 638 days. Univariate analysis showed that patients at a low TNM stage (≤ 3, $P = 0.041$), high *peak* ($P = 0.006$), high ADC$_{min}$ ($P = 0.002$) and low TLG ($P = 0.01$) had better OS. Moreover, high TLG/*peak* ratio was associated with poor OS ($P = 0.016$). Multivariate analysis indicated that ADC$_{min}$ ($P = 0.011$) and TLG/*peak* ratio ($P = 0.006$) were independent predictors of OS after adjustment for age, gender, tumor size, and TNM stage. The TLG/*peak* ratio was an independent predictor of OS in a subgroup of patients who did not receive curative surgery ($P = 0.013$).

✉ Tiffany Ting-Fang Shih
ttfshih@ntu.edu.tw

Bang-Bin Chen
bangbin@gmail.com

Yu-Wen Tien
ywtien5106@ntu.edu.tw

Ming-Chu Chang
mingchuchang@ntu.edu.tw

Mei-Fang Cheng
meifang@ntuh.gov.tw

Yu-Ting Chang
yutingchang@ntu.edu.tw

Shih-Hung Yang
shyang0821@ntuh.gov.tw

Chih-Horng Wu
ared1020@gmail.com

Ting-Chun Kuo
cutytina@hotmail.com

I-Lun Shih
rinkoss@gmail.com

Ruoh-Fang Yen
rfyen@ntu.edu.tw

[1] Department of Medical Imaging and Radiology, National Taiwan University College of Medicine and Hospital, No 7, Chung-Shan South Rd, Taipei 10016, Taiwan

[2] Department of Surgery, National Taiwan University College of Medicine and Hospital, No 7, Chung-Shan South Rd, Taipei 10016, Taiwan

[3] Department of Internal Medicine, National Taiwan University College of Medicine and Hospital, No 7, Chung-Shan South Rd, Taipei 10016, Taiwan

[4] Department of Nuclear Medicine and Radiology, National Taiwan University College of Medicine and Hospital, No 7, Chung-Shan South Rd, Taipei 10016, Taiwan

[5] Department of Oncology, National Taiwan University College of Medicine and Hospital, No 7, Chung-Shan South Rd, Taipei 10016, Taiwan

Conclusion The flow-metabolism mismatch reflected by the TLG/*peak* ratio may better predict OS than other imaging biomarkers from PET/MRI in pancreatic cancer patients.

Introduction

Pancreatic ductal adenocarcinoma (PDAC) is the fourth-most common cause of cancer death [1]. Currently, radical resection of the primary tumor and regional lymphadenectomy are the only potentially curative treatments. Despite recent improvements in adjuvant chemotherapy, patients with PDAC continue to have dismal prognoses: the 5-year overall survival (OS) rate is about 8% [2]. Therefore, identification of novel prognostic biomarkers in patients with PDAC is crucial and can improve the selection of patients for adjuvant therapy and thus, survival outcome.

Because noninvasive imaging biomarkers are used extensively in cancer research [3], positron emission tomography/magnetic resonance imaging (PET/MRI) has shown great potential in tumor diagnosis, treatment planning, surveillance, and follow-up in oncology patients [4–7]. Multiparametric PET/MRI offers various imaging biomarkers for tumor characteristics including blood flow by dynamic contrast-enhanced MRI (DCE-MRI), cellularity by diffusion-weighted imaging (DWI), metabolites by magnetic resonance spectroscopy (MRS), and metabolism by fluorine 18 fluorodeoxyglucose (^{18}F–FDG) in a single examination [6]. Furthermore, these imaging biomarkers can provide novel insights about tumor characteristics and aggressiveness in PDAC.

Among these imaging biomarkers, associations between tumor blood flow-metabolism mismatch and adverse tumor biology have been illustrated in various cancers [8]. Using ^{15}O–H$_2$O and ^{18}F–FDG PET/computed tomography (CT) to quantify blood flow and metabolic activity in pancreatic tumors, a previous study found that high tumor metabolism and low blood flow were linked with an aggressive cancer phenotype and potentially reflect treatment resistance [9]. The flow-metabolism mismatch indicates tumor adaptation to hypoxic stress, and this adaptation could be associated with poorer patient outcomes for PDAC [10–12]. DCE-MRI is a noninvasive technique that can detect tumor blood flow, vascularity, and permeability in vivo and has been used as a functional imaging tool in an integrated PET/MRI examination [6]. Thus, we assume that the correlation between flow and metabolism from DCE-MRI and PET may illustrate tumor aggressiveness and predict outcome in PDAC.

In addition, a positive correlation between high cellularity, reflected by a low apparent diffusion coefficient (ADC) from DWI, and high metabolic activity from ^{18}F–FDG PET has been investigated in many cancers [13–15]. For example, it has recently been reported that in PDAC and periampullary cancer, advanced-stage tumors had lower minimum ADC (ADC$_{min}$) values and higher glucose metabolic activities than did early-stage tumors. And, a high ratio of metabolic tumor volume (MTV)/ADC$_{min}$ was independently associated with shorter progression-free survival (PFS) [16]. Thus, the combined information from multiparametric PET/MRI biomarkers can provide more accurate prognostication about the survival of patients with PDAC.
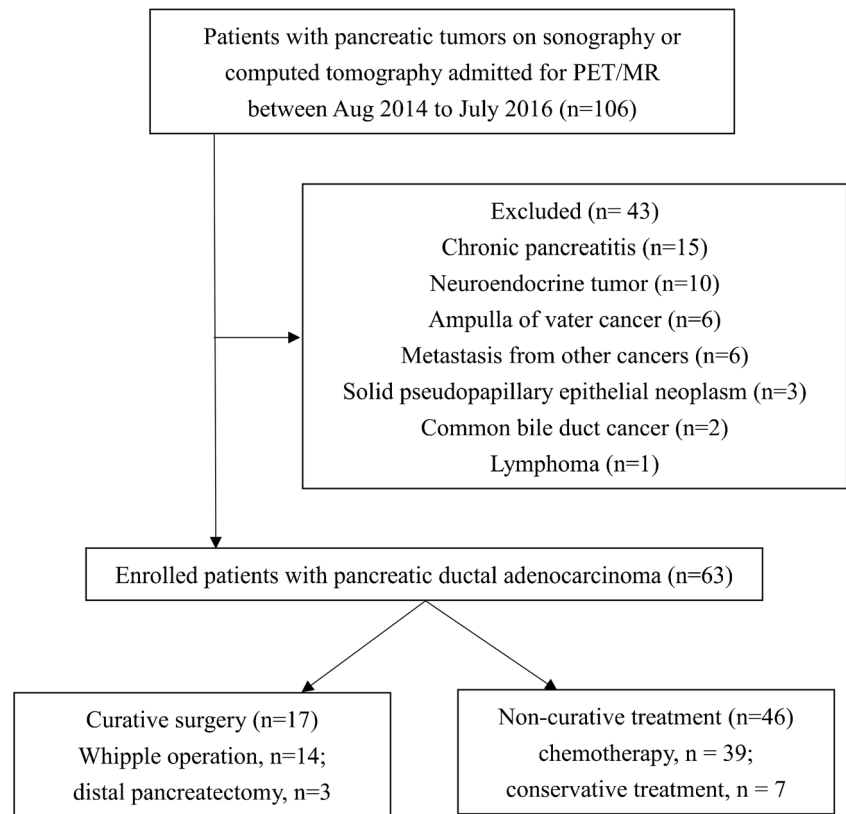
Our hypothesis is that imaging biomarkers from multiparametric PET/MRI before treatment can be used to predict OS in patients with PDAC. The aim of this study was to correlate the OS with the imaging biomarkers of DCE-MRI, DWI, MRS, and glucose metabolic activity derived from integrated PET/MRI in patients with pancreatic cancer.

Materials and methods

Patients

This prospective study was approved by the institutional review board in our hospital, and informed consent was obtained from all patients. From August 2014 to July 2016, 106 consecutive patients were admitted for examination by PET/MRI before treatment. Inclusion criteria were suspicious pancreatic cancer on sonography or CT and no local or systemic treatments. Exclusion criteria were pregnancy and contraindications for 3-T MRI. All patients were pathology-proven by surgery, endoscopic ultrasound, or CT-guided biopsy. Tumor size, histological grade, and lymph node metastasis were recorded. Finally, 63 patients (mean age, 62.7 ± 12 y; range, 34–83 y; 40 men, 23 women) with PDAC comprised our study population after excluding 43 patients with chronic pancreatitis ($n = 15$) or other malignancy ($n = 28$) (Fig. 1). All patients tolerated this examination. Patient characteristics are presented in Table 1.

Some patients participated in another study [16] that analyzed associations between imaging biomarkers from DWI, MRS, and PET with tumor grade, clinical stage, and PFS in patients with PDAC or periampullary cancer. In this study, we focus primarily on associations between imaging biomarkers and OS in patients with PDAC, and we include imaging

Fig. 1 Flow diagram of enrolled patients

Patients with pancreatic tumors on sonography or computed tomography admitted for PET/MR between Aug 2014 to July 2016 (n=106)

Excluded (n= 43)
Chronic pancreatitis (n=15)
Neuroendocrine tumor (n=10)
Ampulla of vater cancer (n=6)
Metastasis from other cancers (n=6)
Solid pseudopapillary epithelial neoplasm (n=3)
Common bile duct cancer (n=2)
Lymphoma (n=1)

Enrolled patients with pancreatic ductal adenocarcinoma (n=63)

Curative surgery (n=17)
Whipple operation, n=14;
distal pancreatectomy, n=3

Non-curative treatment (n=46)
chemotherapy, n = 39;
conservative treatment, n = 7

biomarkers from DCE-MRI. Neither DCE-MRI nor OS data have been reported previously.

PET/MRI protocol

Whole-body PET/MRI was performed using an integrated PET/MRI system (Biograph mMR; Siemens Healthcare, Erlangen, Germany). Approximately 60 min after injection of FDG (5.18 MBq/kg) and bladder evacuation, PET was performed from the head to the mid-thighs in five bed positions (acquisition time, 4 min/position) with the patient in a supine arm-down position. Images were reconstructed using an ordered-subsets expectation maximization iterative algorithm (two iterations, 21 subsets) with a 5-mm post-reconstruction Gaussian filter and a 172×172 image matrix. Attenuation correction of the PET data was performed using a 4-tissue-class (air, lung, fat, and soft tissue) segmented attenuation map acquired using a 2-point Dixon MRI sequence. Simultaneous MRI with coronal and axial T2-weighted half-Fourier single-shot turbo spin-echo sequences was performed while acquiring PET data at each bed position. Beyond MRI acquisition protocol, PET information was strictly linked to the employed beta-emitting tracer.

Following simultaneous PET and MRI acquisition, axial T1-weighted imaging with a 2-D fast low-angle shot and axial T2-weighted imaging with fat suppression were performed on the abdomen (Table 2).

DCE-MRI

DCE-MRI was performed using a 3-D gradient-echo sequence with isotropic resolution in three dimensions. A T1 map of the pancreas was initially created using various flip angles (5°, 10°, 15°, and 20°) to establish baseline T1 values. A MR pulse sequence with a T1-weighted volumetric interpolated breath-hold examination (3.17-s temporal resolution per volume) was started 50 s prior to injection of gadobutrol (0.05 mmol/kg, Gadovist® 1.0; Schering, Berlin, Germany) at a flow of 3 mL/s. Baseline images were acquired 10 s (10 phases) before initiating contrast agent injection. All patients were instructed to suspend breathing for as long as possible, then breathe slowly and smoothly during imaging. Imaging time was 3 min, 57 s to obtain 90 volumes (1260 images).

DWI

Pulse sequences included an axial diffusion-weighted echo-planar imaging sequence with free breathing. The ADC map was calculated using a monoexponential function (b-values, 0, 600, and 1000 s/mm^2) [16].

MRS

Single-voxel MRS data were acquired using a point-resolved selective spectroscopy sequence and standard parameters

Table 1 Clinical information of the 63 patients with pancreatic cancers

Age (years) *	62.7 ± 12 (34~83)
Gender (M/F) *	40/23
Tumor size (cm) *	3.4 ± 1.5
Glucose (mg/dL) *	117 ± 41
FDG (MBq) *	371 ± 86.6
CEA (ng/ml) *	6.2 (0.4~5783)
CA19–9 (U/ml) *	221 (1.5~26,000)
Tumor location†	
Head	33 (52)
Neck	8 (13)
Body	16 (25)
Tail	6 (10)
Surgery method† ($n = 21$)	
Whipple operation	14
Distal pancreatectomy	3
Exploratory laparotomy and biopsy	2
Bypass and biopsy	2
TNM staging†	
I	4 (6)
II	13 (21)
III	9 (14)
IV	37 (59)
Histology grade† ($n = 22$)	
Well-differentiated	3
Moderately differentiated	9
Poorly differentiated	10

*Data are means ± standard deviations or median values, with range in parentheses

†Data are numbers of patients, with percentages in parentheses

FDG: Fluorine 18 fluorodeoxyglucose

CEA: serum carcinoembryonic antigen

CA19–9: carbohydrate antigen 19–9

(1000/30 ms TR/TE; 90° flip angle) during free-breathing. Automated optimization of transmitter pulse power, localized shimming, gradient tuning, and water suppression were used. Data were acquired at a spectral bandwidth of 1200 Hz, and 200 signals were averaged for each water-suppressed spectrum [16].

Post-contrast multiphasic and whole-body MRI

Finally, multiphasic (arterial, portovenous, and equilibrium phases) T1-weighted imaging of the pancreas was performed using gadobutrol (0.05 mmol/kg), and contrast-enhanced imaging of the whole body was performed using an axial volumetric interpolated breath-hold examination sequence. Magnetic resonance cholangiopancreatography was also performed. The total length of the PET/MRI examination was approximately 60 min per participant (Figs. 2 and 3).

Image analysis

One radiologist (B.B.C., with 12 years of experience in abdominal imaging) measured the DCE-MRI, DWI, MRS, and PET parameters of the pancreatic tumor. One nuclear medicine physician (M.F.C., with 14 years of experience) evaluated the lymph nodes and distant metastases on PET/MRI. The radiologist and nuclear medicine physician independently performed their parts on the workstation.

The TNM stages (American Joint Committee on Cancer, 7th edition) of study patients were determined by a multidisciplinary team for pancreatic cancer at our hospital. In those who did not receive curative surgery, stage was determined by biopsy and all available image results.

The DCE-MRI data were analyzed using a commercial software tool (MIStars; Apollo Medical Imaging, Melbourne, Australia) [17]. Motion correction was performed using a 2-D rigid body registration. Two semi-quantitative parameters (*peak* and $IAUC_{60}$) were derived. The former was defined as $(SI_{max} - SI_{base})/SI_{base} * 100$, where SI_{base} represents the average baseline signal before the arrival of contrast agent in the arteries, and SI_{max} represents the maximum value of the first pass of the time-signal intensity curve. The latter was the area under the curve for the first 60 s after contrast material arrived in the region of interest (ROI). Three quantitative parameters (volume transfer constant [K^{trans}], reflux constant [k_{ep}], and extra-vascular extra-cellular volume fraction [v_e]) were derived using a bicompartmental model [18] and nonlinear fitting of the individual time-intensity curve. Regions of interest were manually drawn on the abdominal aorta at the level of the celiac axis for the arterial input function. These parameters were automatically calculated pixel-by-pixel using a constrained nonlinear least-squares fitting algorithm with adjustable delay time [17]. The mean ROI size was 4.9 ± 4.6 cm^2 (range, 0.6–25.6 cm^2).

To measure the ADC, ROIs were manually drawn on the ADC map along the contour of the tumor on the single slice containing the largest area of the tumor. The lowest ADC value in an ROI, ADC_{min}, represented the greatest tumor cellularity. The mean ROI size was 8.7 ± 6.6 cm^2 (range, 0.6–28.4 cm^2).

In MRS, post-processing, zero filling, Fourier transformation, and phase correction were implemented. The volumes of interest were 3.6 ± 1.3 cm^3 (range, 3.4–12.5 cm^3). The area of the choline peak at 3.2 ppm was calculated using Syngovia software. MRS was successful in 56 patients.

Relevant PET-related parameters were SUV_{max}, which reflects the maximum standardized uptake value (adjusted for body weight); SUV_{mean}, which reflects average SUVs; MTV, expressed as the tumor volume with FDG uptake, which was segmented using a fixed-percentage threshold method at 50% of the SUV_{max}; and total lesion glycolysis (TLG), representing the product of MTV and the average SUVs of the included

Table 2 Parameters of PET/MRI examination

Sequence	Repetition time (msec)	Echo time (msec)	Flip angle (°)	Matrix	Field of view (mm)	Slice thickness /gap (mm)	NEX	Acquisition time (min:sec)
During PET								
Coronal T2WI	1240	87	90	384× 258	450× 302	6/0.6	1	2:37
Axial T2WI	1000	85	90	320× 260	350× 284	6/0	1	3:14
After PET								
Axial T1WI	138	2.5	70	640× 240	300× 253	5/0	1	0:42
Axial T2WI	2000	97	121	640× 496	300× 233	5/0	1	1:30
DCE-MRI	4.7	2.5	15	192× 168	340× 298	5/0	1	3:57
DWI	7500	83	90	312× 216	350× 242	5	3	3:00
MRCP	1500	85	90	512× 496	260× 252	4/0	1	1:18
Dynamic axial T1WI post-contrast	3.3	1.2	15	265× 224	320× 280	1.8/0	1	0:22 (3 sets)
Whole-body axial T1WI post-contrast	3.3	1.2	15	256× 192	370× 298	3/0	1	2:24

T2WI: T2-weighted images; FLAIR: fluid-attenuated inversion recovery images; T1WI: T1-weighted images; DCE-MRI: dynamic contrast-enhanced magnetic resonance image; DWI: diffusion weighted imaging; MRCP: magnetic resonance cholangiopancreatography; NEX: Number of excitations
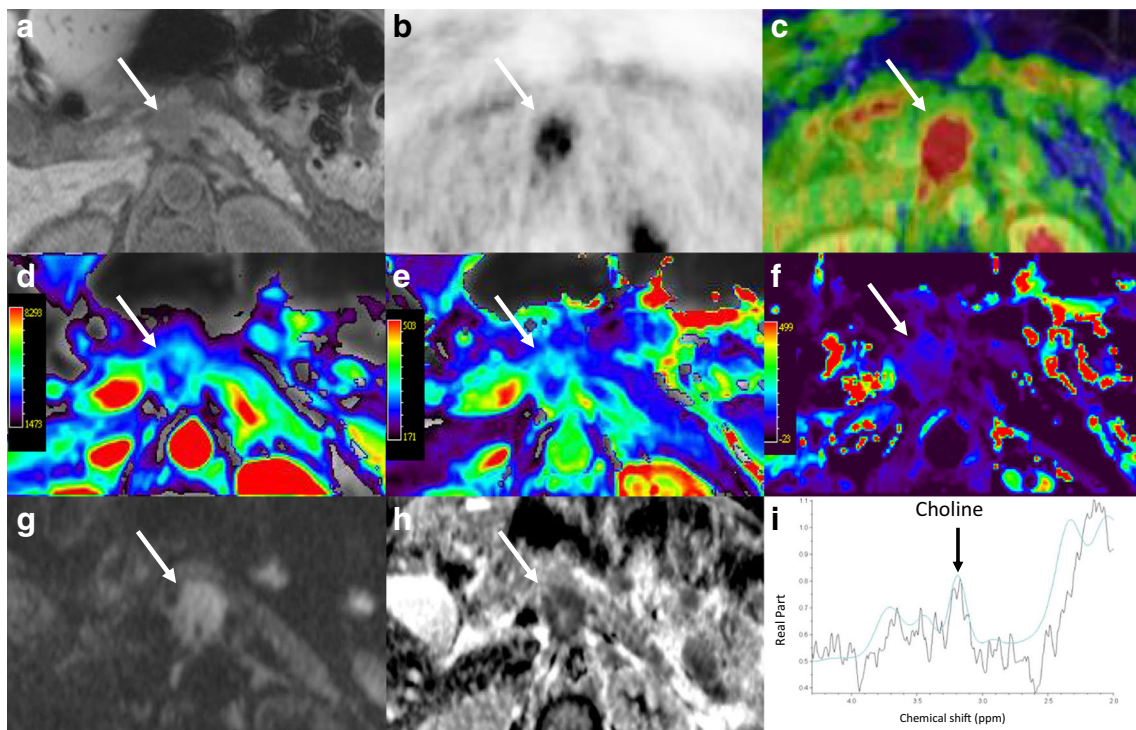

Fig. 2 Images of a 56-year-old man with pancreatic head cancer (arrow) (T4N1M1). (**a**) Pre-contrast T1-weighted MR (**b**) PET (**c**) fused PET/venous phase CE T1-weighted VIBE MR. (**d–f**) DCE-MRI color maps: (**d**) $IAUC_{60}$ (**e**) $peak$ (**f**) K^{trans} (**g**) diffusion-weighted image (b = 1000) (**h**) ADC map (**i**) MR spectroscopy. This patient underwent chemotherapy and overall survival was 199 days
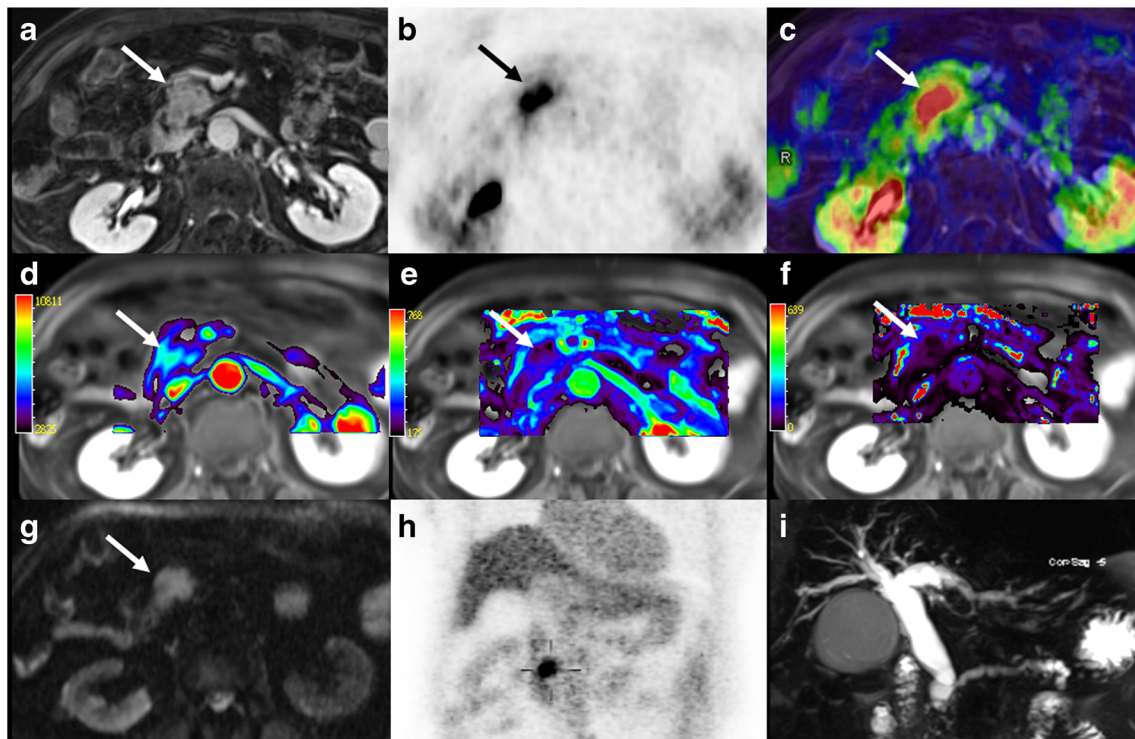
Fig. 3 Images of a 76-year-old man with pancreatic head cancer (arrow) (T1N1M0). (**a**) Venous phase CE T1-weighted MR (**b**) axial PET (**c**) fused PET/venous phase CE T1-weighted MR. (**d–f**) DCE-MRI color maps: (**d**) $IAUC_{60}$ (**e**) *peak* (**f**) K^{trans} (**g**) diffusion-weighted image (b = 1000) (**h**) coronal PET (**i**) MR cholangiopancreatography shows marked dilatation of common bile duct and main pancreatic duct. This patient underwent Whipple operation and overall survival was 638 days

Table 3 Pearson correlations among PET/MR imaging biomarkers

Parameters		*peak*	$IAUC_{60}$	K^{trans}	k_{ep}	v_e
ADC_{min}	Correlation (*r*)	0.258	−0.002	0.032	0.179	−0.138
	P value	0.024*	0.495	0.405	0.087	0.148
Choline	Correlation (*r*)	0.053	0.008	0.368	0.357	0.245
	P value	0.350	0.475	0.003**	0.003**	0.034*
SUV_{max}	Correlation (*r*)	−0.003	0.183	−0.298	−0.139	−0.235
	P value	0.491	0.076	0.009**	0.139	0.032*
SUV_{mean}	Correlation (*r*)	−0.02	0.02	−0.076	0.137	−0.108
	P value	0.437	0.438	0.277	0.142	0.2
MTV	Correlation (*r*)	−0.331	−0.33	−0.085	−0.094	−0.094
	P value	0.004**	0.004**	0.254	0.232	0.232
TLG	Correlation (r)	−0.302	−0.213	−0.1	0.007	−0.120
	P value	0.008**	0.047*	0.219	0.478	0.174
Size	Correlation (r)	−0.395	−0.081	−0.270	−0.174	−0.209
	P value	0.001**	0.265	0.016*	0.086	0.05*

peak = (maximum signal – baseline signal) / baseline signal; $IAUC_{60}$ = initial area under the curve for the first 60 s after contrast material arrival; K^{trans} = forward volume transfer constant; k_{ep} = reverse volume transfer constant; v_e = extravascular extracellular space volume per unit volume of tissue; ADC_{min} = minimum apparent diffusion coefficient; SUV_{max} = maximum standardized uptake value; SUV_{mean} = mean standardized uptake value; MTV = metabolic tumor volume; TLG = total lesion glycolysis

* indicates $P < 0.05$

** indicates $P < 0.01$

Table 4 Differences in DCE-MRI parameters and TLG/*peak* ratio relative to pathological grades and TNM stage

Parameter		peak (%)	$IAUC_{60}$ (/100, sec)	K^{trans} (min^{-1}/ 1000)	k_{ep} (min^{-1}/ 1000)	v_e (%/10)	TLG/ peak
Tumor differentiation (n = 22)	Well-moderate (n = 12)	333 ± 42	402 ± 216	61 ± 95	417 ± 491	106 ± 128	9.2 ± 7.6
	Poor (n = 10)	327 ± 96	426 ± 241	14 ± 19	201 ± 254	32 ± 31	12 ± 11
	P value	0.582	0.771	0.093	0.159	0.059	0.674
T-stage (N = 63)	≦3 (n = 29)	325 ± 71	436 ± 223	43 ± 70	358 ± 354	85 ± 101	12 ± 9
	4 (n = 34)	287 ± 64	393 ± 226	43 ± 80	348 ± 567	78 ± 105	37 ± 75
	P value	0.039*	0.473	0.199	0.253	0.336	0.002*
N-stage (N = 63)	0 (n = 15)	324 ± 59	390 ± 268	51 ± 85	508 ± 771	90 ± 119	9 ± 7
	1 (n = 48)	298 ± 72	420 ± 211	41 ± 72	304 ± 336	78 ± 98	30 ± 64
	P value	0.076	0.561	0.656	0.453	0.695	0.007*
N-stage† (n = 17)	0 (n = 8)	350 ± 30	363 ± 230	75 ± 110	435 ± 362	135 ± 149	5 ± 3
	1 (n = 9)	334 ± 87	509 ± 147	25 ± 42	326 ± 518	43 ± 33	9 ± 5
	P value	0.2	0.2	0.0236*	0.277	0.2	0.114
M-stage (N = 63)	0 (n = 26)	323 ± 74	418 ± 215	42 ± 71	372 ± 410	76 ± 95	14 ± 21
	1 (n = 37)	292 ± 64	417 ± 233	44 ± 78	340 ± 524	84 ± 109	33 ± 71
	P value	0.058	0.955	0.726	0.463	0.582	0.002*
TNM stage (N = 63)	≦2 (n = 17)	339 ± 76	444 ± 201	49 ± 82	402 ± 424	89 ± 110	9 ± 8
	>2 (n = 46)	292 ± 64	402 ± 233	41 ± 73	334 ± 499	78 ± 101	31 ± 65
	P value	0.01*	0.394	0.241	0.239	0.202	<0.001*

peak = (maximum signal – baseline signal) / baseline signal; $IAUC_{60}$ = initial area under the curve for the first 60 s after contrast material arrival; K^{trans} = forward volume transfer constant; k_{ep} = reverse volume transfer constant; v_e = extravascular extracellular space volume per unit volume of tissue

†A subgroup of patients (n = 17) who received curative surgery with lymph node dissection. The pathological findings are used as the gold standard

* indicates $P < 0.05$

voxels. The fixed-threshold MTV and TLG were automatically derived from these tumor delineations by the software (available as a predefined Syngovia tool) [16].

Excellent inter-observer reliability has been reported for ADC_{min}, SUV_{max}, SUV_{mean}, TLG, and MTV [16].

Statistical analysis

Summary statistics are presented as the mean (± standard deviation [SD]) for continuous variables, or frequency and percentage for categorical variables. Pearson correlation coefficients (r) were calculated to evaluate the relationships between imaging biomarkers and tumor size. Differences in the DCE-MRI imaging biomarkers relative to tumor grade and TNM stages were compared using the Mann–Whitney test. The TNM stages were based on surgical or imaging findings. For the nodal stage, a subgroup of patients (n = 17) who received curative surgery with lymph node dissection was also analyzed, and pathological findings were used as the gold standard.

OS was measured from the date of the first MR exam to the date of death or study completion (June 30, 2017). Time to

progression (TTP) was defined as the time from the first MR exam to the time of tumor progression. For survival analysis, each variable was dichotomized as either high or low based on the median value of the variable. The Kaplan-Meier method was used to plot survival curves, and the two-sided log-rank test was used to assess differences in OS and TTP between patient groups. Multivariable analysis was investigated using the step-wise forward Cox proportional hazard model with the variables age, tumor size, TNM stage, and imaging biomarkers. A subgroup analysis of patients without curative surgery was also performed. Data were analyzed using SPSS software (SPSS for Windows 22; IBM Corp., Armonk, NY, USA). Significance was recognized when $P < 0.05$.

Results

Clinical treatment and follow-up

Of 63 patients, 39 (62%) died during this study. All patients died of pancreatic cancer, so the disease-specific OS and general survival were the same in our study cohort. Median

Fig. 4 Kaplan–Meier survival curves show that patients with low values of (**a**) *peak* or (**b**) minimum ADC (ADC$_{min}$) have shorter overall survival than those with high values. Patients with high values of (**c**) total lesion glycolysis (TLG) or (**d**) TLG/*peak* ratio have shorter overall survival than those with low values
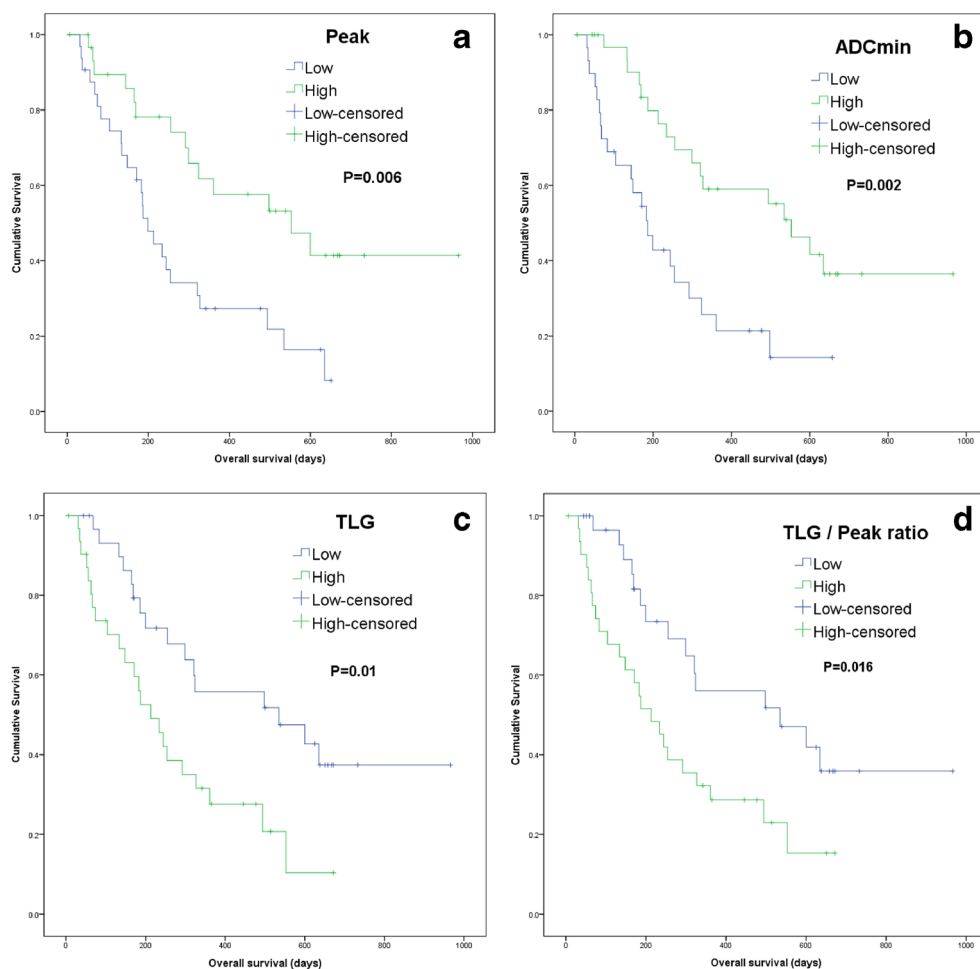
survival was 234 days (range, 6–966 days), and median follow-up was 638 days. Fifty-four patients (85.7%) had disease progression during follow-up and median TTP was 89 days (range, 6–966 days). Seventeen (17/63, 27%) patients received curative surgery (Whipple operation, $n = 14$; distal pancreatectomy, $n = 3$), and 15 received adjuvant chemotherapy. In 46 patients who did not receive curative surgery, 39 received chemotherapy, and seven received conservative treatment. Those who did not receive curative surgery had a much shorter OS than those who did (median survival 244 vs. 635 days, $P = 0.012$).

Correlations between PET/MRI biomarkers and tumor size

Values for *peak* were positively correlated with ADC$_{min}$ ($r = 0.258$, $P = 0.024$). Choline was positively correlated with K^{trans} ($r = 0.368$, $P = 0.003$), k_{ep} ($r = 0.357$, $P = 0.003$), and v_e ($r = 0.234$, $P = 0.034$). In contrast, SUV$_{max}$ was negatively correlated with K^{trans} ($r = -0.298$, $P = 0.009$) and v_e ($r = -0.235$, $P = 0.032$). Both *peak* and $IAUC_{60}$ were negatively

correlated with MTV and TLG (all $P < 0.05$). Large tumors had lower values for *peak*, K^{trans}, and v_e than small tumors (all $P < 0.05$; Table 3).

Association between imaging biomarkers and pathologic grade, TNM stage

Among DCE-MRI biomarkers, *peak* was lower in tumors with T4 (T4 vs. T≦3, $P = 0.039$) and higher TNM stage (stage >2 vs. ≦2, $P = 0.01$) than in lower-stage tumors. The ratio TLG/*peak* was higher for tumors with T4 (T4 vs. T≦3, $P = 0.002$), N1 (N1 vs. N0, $P = 0.007$), M1 (M1 vs. M0, $P = 0.002$), or higher TNM stage (stage >2 vs. ≦2, $P < 0.001$) than in lower-stage tumors (Table 4).

Relationships between imaging biomarkers and OS in all patients

Univariate analyses revealed that advanced stage ($P = 0.041$; hazard ratio [HR] = 2.041, 95% confidence interval [CI] = 1.029–4.048), low *peak* ($P = 0.006$; HR = 2.559, 95% CI =

Table 5 Correlation of imaging biomarkers with overall survival in all 63 patients

Parameters	Cutoff	Univariate			Multivariate		
		HR	95% CI	P value	HR	95% CI	P value
Age (years)	64	1.13	0.6–2.127	0.706			
Gender (female vs. male)		0.629	0.322–1.23	0.175			
Size (cm) ($\leq$3.3 vs. >3.3)	3.3	0.777	0.413–1.46	0.433			
TNM stage (4 vs.$\leq$3)		2.041	1.029–4.048	0.041[*]			
Imaging biomarkers							
$peak$ (%)	297	2.559	1.315–4.981	0.006[*]			
$IAUC_{60}$ (/100, sec)	399	1.279	0.68–2.405	0.445			
K^{trans} (min^{-1}/1000)	7	1.392	0.735–2.638	0.310			
k_{ep} (min^{-1}/1000)	213	1.288	0.680–2.439	0.437			
v_e (%/10)	27	1.066	0.564–2.015	0.844			
ADC_{min} (10^{-6} mm^2/s)	844	2.861	1.477–5.543	0.002[*]	0.999	0.998–1	0.011[*]
Choline	3.33	1.210	0.615–2.378	0.581			
SUV_{max} (g/mL)	7.2	0.985	0.525–1.846	0.961			
SUV_{mean} (g/mL)	4.46	0.985	0.525–1.846	0.961			
MTV (cm^3)	8.54	0.577	0.305–1.09	0.09			
TLG (g)	33	0.421	0.217–0.816	0.01[*]			
TLG/$peak$	11.81	0.444	0.230–0.858	0.016[*]	4.610	1.565–13.582	0.006[*]

HR = hazard ratio; CI = confidence interval; $peak$ = (maximum signal − baseline signal) / baseline signal; $IAUC_{60}$ = initial area under the curve for the first 60 s after contrast material arrival; K^{trans} = forward volume transfer constant; k_{ep} = reverse volume transfer constant; v_e = extravascular extracellular space volume per unit volume of tissue; ADC_{min} = minimum apparent diffusion coefficient; SUV_{max} = maximum standardized uptake value; SUV_{mean} = mean standardized uptake value; MTV = metabolic tumor volume; TLG = total lesion glycolysis

The multivariate analysis includes continuous variables (age, tumor size, $peak$, ADC_{min}, TLG, TLG/$peak$) and categorical variables (gender and TNM stage)

* indicates P value is significant <0.05

Table 6 Correlation of imaging biomarkers with overall survival in a subgroup of 46 patients without curative surgery

OS	Univariate			Multivariate		
Parameters	HR	95% CI	P value	HR	95% CI	P value
Age	0.993	0.964–1.023	0.654			
Gender	0.502	0.242–1.042	0.064			
Size	1.019	0.786–1.32	0.887			
TNM stage (4 vs.$\leq$3)	1.061	0.477–2.359	0.885			
Image biomarkers						
$peak$	0.993	0.988–0.999	0.021[*]			
ADC_{min}	0.999	0.998–1	0.019[*]			
TLG	1.005	1.002–1.009	0.004[*]			
TLG/$peak$	4.682	1.426–15.374	0.011[*]	4.573	1.373–15.236	0.013[*]

HR = hazard ratio; CI = confidence interval; $peak$ = (maximum signal − baseline signal) / baseline signal; ADC_{min} = minimum apparent diffusion coefficient; TLG = total lesion glycolysis

The continuous variables of imaging biomarkers are used in the univariate analysis. The multivariate analysis includes continuous variables (age, tumor size, $peak$, ADC_{min}, TLG, TLG/$peak$) and categorical variables (gender and TNM stage)

* indicates P value is significant <0.05

Table 7 Correlation of imaging biomarkers with time to progression in all 63 patients

Parameters	Cutoff	Univariate			Multivariate		
		HR	95% CI	P value	HR	95% CI	P value
Age (years)	64	1.06	0.62–1.812	0.832			
Gender (female vs. male)		1.165	0.671–2.022	0.587			
Size (cm) ($\leqq$3.3 vs. >3.3)	3.3	0.671	0.392–1.148	0.145			
TNM stage (4 vs.$\leqq$3)		1.748	1.011–3.023	0.045[*]			
Imaging biomarkers							
$peak$ (%)	297	1.697	0.987–2.916	0.056			
$IAUC_{60}$ (/100, sec)	399	1.185	0.694–2.203	0.533			
K^{trans} (min^{-1}/1000)	7	1.492	0.871–2.555	0.145			
k_{ep} (min^{-1}/1000)	213	1.043	0.611–1.780	0.878			
v_e (%/10)	27	1.143	0.669–1.955	0.624			
ADC_{min} (10^{-6} mm^2/s)	844	1.694	0.988–2.906	0.056			
Choline	3.33	1.432	0.811–2.527	0.216			
SUV_{max} (g/mL)	7.2	0.825	0.482–1.408	0.48			
SUV_{mean} (g/mL)	4.46	0.825	0.482–1.408	0.48			
MTV (cm^3)	8.54	0.6	0.350–1.027	0.062			
TLG (g)	33	0.454	0.263–0.781	0.004[*]	1.004	1.001–1.007	0.012[*]
TLG/$peak$	11.81	0.402	0.233–0.694	0.001[*]	2.130	1.158–3.915	0.015[*]

HR = hazard ratio; CI = confidence interval; $peak$ = (maximum signal − baseline signal) / baseline signal; $IAUC_{60}$ = initial area under the curve for the first 60 s after contrast material arrival; K^{trans} = forward volume transfer constant; k_{ep} = reverse volume transfer constant; v_e = extravascular extracellular space volume per unit volume of tissue; ADC_{min} = minimum apparent diffusion coefficient; SUV_{max} = maximum standardized uptake value; SUV_{mean} = mean standardized uptake value; MTV = metabolic tumor volume; TLG = total lesion glycolysis

The multivariate analysis includes continuous variables (age, tumor size, $peak$, ADC_{min}, TLG, TLG/$peak$) and categorical variables (gender and TNM stage)

* indicates P value is significant <0.05

1.315–4.981, Fig. 4a), low ADC_{min} (P = 0.002; HR = 2.861, 95% CI = 1.477–5.543, Fig. 4b), and high TLG (P = 0.01; HR = 3.511, 95% CI = 1.182–10.429, Fig. 4c) were prognostic factors for poor OS. In addition, a high metabolism-to-flow ratio (TLG/$peak$ [P = 0.016; HR = 3.511, 95% CI = 1.182–10.429]) was a prognostic factor for poor OS (Fig. 4d). Cox multivariate analysis revealed that TLG/$peak$ (P = 0.006; HR = 4.61, 95% CI = 1.565–13.582) and ADC_{min} (P = 0.011; HR = 0.999, 95% CI = 0.998–1) remained independent predictors of OS after adjusting for age, gender, tumor size, TNM stage, and other imaging biomarkers (Table 5).

Relationships between imaging biomarkers and OS in patients without curative surgery

Because curative surgery was an important prognostic factor for OS, we further performed subgroup analyses using the 46 patients who did not receive curative surgery to determine the prognostic values for these imaging biomarkers.

Similarly, univariate analyses revealed that $peak$, ADC_{min}, TLG, and TLG/$peak$ were prognostic factors (all P < 0.05). Only the final factor was significant in multivariate analyses after adjustment for age, gender, tumor size, TNM stage, and other imaging biomarkers (P = 0.013; HR = 4.573, 95% CI = 1.373–15.236) (Table 6). Therefore, TLG/$peak$ was the best predictor for OS in patients who did not receive curative surgery.

Relationships between imaging biomarkers and TTP in all patients

Univariate analyses revealed that advanced stage (P = 0.045; HR = 1.748, 95% CI = 1.011–3.023), high TLG (P = 0.004; HR = 2.205, 95% CI = 1.280–3.797), high TLG/$peak$ (P = 0.001; HR = 2.489, 95% CI = 1.441–4.3) were prognostic factors for shorter TTP. Cox multivariate analysis revealed that TLG (P = 0.012) and TLG/$peak$ (P = 0.015) remained independent predictors of TTP after adjusting for age, gender, tumor size, TNM stage, and other imaging biomarkers (Table 7).

Discussion

In this study, we found that high *peak*, high ADC_{min}, and low TLG were good prognostic predictors of OS in patients with PDAC. The TLG/*peak ratio* and ADC_{min} were independent predictors after controlling for age, gender, size, and stage. In patients who did not receive curative surgery, the former remained an independent predictor for OS. Besides, both high TLG and TLG/*peak* ratio were independent predictors for shorter TTP as well.

The parameters of DCE-MRI have been found to correlate with tumor angiogenesis, degree of tumor fibrosis, expression of vascular endothelial growth factor Ki67, and microvascular density in PDAC [19, 20]. Compared to normal pancreas, those affected by PDAC were found to have lower values for *IAUC*, K^{trans}, and k_{ep}, and larger values for v_e [21, 22], suggesting decreased blood flow and increased interstitial space within the tumors. In this study, tumors with low *peak* values were associated with advanced TNM stage and poor OS. This variable is a semi-quantitative parameter and represents a combination of blood flow, interstitial volume, and tumor permeability [17]. We assume that the abundant fibrous stroma in more aggressive tumors impede blood flow, leading to intratumoral hypoxia and impaired drug delivery. Therefore, tumors with low *peak* values were associated with poor prognoses. Also, a previous study found that tumors with low values for K^{trans} and k_{ep} were associated with poor responses after antiangiogenic therapy [23]. Based on these results, it seems that high tumor angiogenesis before treatment is associated with better therapy response and survival outcome in PDAC.

DWI can potentially depict and characterize a variety of focal pancreatic lesions [24], particularly for staging in PDAC [25]. The ADC is significantly lower in tumors with dense fibroses and can serve as a biomarker of fibrosis architecture [26, 27]. Previous studies showed that a low pretreatment ADC was associated with shorter PFS after chemotherapy [28] and shorter OS in patients with resected PDAC [29]. We found that a low pretreatment ADC_{min} independently predicted a poor outcome in all patients and also in the subgroup of patients without curative surgery. We also found a positive correlation between ADC_{min} and *peak*, suggesting reduced blood flow in tumors with high cellularity or abundant fibroses. Further studies are needed to evaluate the usefulness of DWI for monitoring treatment.

Using ^1H–MRS, we found that choline was positively correlated with K^{trans}, k_{ep}, and v_e. In PDAC, increased levels of choline suggest increased membrane activity, particularly enhanced cellular proliferation. In vivo, poor perfusion can limit substrate delivery, thus decreasing metabolite concentrations in poorly vascularized regions of the tumor [30]. Although a previous study found that low choline was associated with longer survival in PDAC [31], we did not find it was associated with OS, likely because the patient sample in this study was small.

Several studies have shown the potential role of PET in determining therapy response, recurrence detection, and survival prediction [32]. This study confirms that high TLG indicates poor OS and TTP. Tumor blood flow and glucose metabolism are correlated with each other because when blood flow decreases, tumor hypoxia promotes gene expression via the transcription factor hypoxia-inducible factor-1α, which leads to accelerated glycolysis [33]. When more highly expressed, it might promote inflammation and fibrosis in PDAC [34], and it has been shown to correlate with poor prognoses in these patients [35]. Therefore, the combined flow-metabolism imaging biomarker, TLG/*peak*, outperforms other imaging biomarkers in predicting OS, even in patients without curative surgery. This biomarker could be obtained in a single study via integrated PET/MRI in clinical practice, and it is potentially a biomarker for monitoring therapy response.

Several studies have found correlations between imaging biomarkers and tumor histologic findings such as microvascular density, fibrosis, and nuclear grade [16, 27, 36]. In this study, v_e seems to be lower in poorly differentiated PDAC compared to well- to moderately differentiated tumors ($P = 0.059$), but further studies with larger sample sizes are needed.

We acknowledge some limitations in this study. First, the number of patients is limited, especially among those who received curative surgery. Because PDAC is extremely aggressive, very few patients are treated with curative surgery. Second, further studies should take into account additional elements that affect patient survival, such as performance status. Third, a comparative effectiveness study should be performed to evaluate serum markers versus imaging biomarkers. Fourth, ADC_{min} and SUV_{max} are essentially single data points and could be influenced by image noise. Our findings should be validated with multicenter studies. Another limitation of this study is the long duration of the PET/MRI acquisition protocol for multiparametric imaging. According to our results, MRS could be omitted to reduce examination time in clinical practice because choline was not correlated with survival outcome.

In conclusion, multiparametric PET/MRI biomarkers are associated with OS and TTP in patients with PDAC. These prognostic biomarkers might be useful for the design and development of future trials or the selection of personalized therapeutic options, possibly changing the management and improving the prognosis for patients with PDAC.

Compliance with ethical standards

Conflict of interest None.

Ethical approval All procedures performed in studies involving human participants were in accordance with the ethical standards of the

institutional and national research committee and with the 1964 Helsinki declaration and its later amendments or comparable ethical standards.

Informed consent   Informed consent was obtained from all individual participants included in the study.

References

1. Ryan DP, Hong TS, Bardeesy N. Pancreatic adenocarcinoma. N Engl J Med. 2014;371:2140–1. https://doi.org/10.1056/NEJMc1412266.
2. Siegel RL, Miller KD, Jemal A. Cancer statistics, 2017. CA Cancer J Clin. 2017;67:7–30. https://doi.org/10.3322/caac.21387.
3. O'Connor JP, Aboagye EO, Adams JE, Aerts HJ, Barrington SF, Beer AJ, et al. Imaging biomarker roadmap for cancer studies. Nat Rev Clin Oncol. 2017;14:169–86. https://doi.org/10.1038/nrclinonc.2016.162.
4. Rosenkrantz AB, Friedman K, Chandarana H, Melsaether A, Moy L, Ding YS, et al. Current status of hybrid PET/MRI in oncologic imaging. AJR Am J Roentgenol. 2016;206:162–72. https://doi.org/10.2214/AJR.15.14968.
5. Torigian DA, Zaidi H, Kwee TC, Saboury B, Udupa JK, Cho ZH, et al. PET/MR imaging: technical aspects and potential clinical applications. Radiology. 2013;267:26–44. https://doi.org/10.1148/radiol.13121038.
6. Wang J, Shih TT, Yen RF. Multiparametric evaluation of treatment response to Neoadjuvant chemotherapy in breast cancer using integrated PET/MR. Clin Nucl Med. 2017;42:506–13. https://doi.org/10.1097/RLU.0000000000001684.
7. Joo I, Lee JM, Lee DH, Lee ES, Paeng JC, Lee SJ, et al. Preoperative assessment of pancreatic cancer with FDG PET/MR imaging versus FDG PET/CT plus contrast-enhanced multidetector CT: a prospective preliminary study. Radiology. 2017;282:149–59. https://doi.org/10.1148/radiol.2016152798.
8. Miles KA, Williams RE. Warburg revisited: imaging tumour blood flow and metabolism. Cancer Imaging : Off Publ Int Cancer Imaging Soc. 2008;8:81–6. https://doi.org/10.1102/1470-7330.2008.0011.
9. Komar G, Kauhanen S, Liukko K, Seppanen M, Kajander S, Ovaska J, et al. Decreased blood flow with increased metabolic activity: a novel sign of pancreatic tumor aggressiveness. Clin Canc Res : Off J Am Assoc Canc Res. 2009;15:5511–7. https://doi.org/10.1158/1078-0432.CCR-09-0414.
10. Michalski CW, Erkan M, Friess H, Kleeff J. Tumor metabolism to blood flow ratio in pancreatic cancer: helpful in patient stratification? Future Oncol. 2010;6:13–5. https://doi.org/10.2217/fon.09.151.
11. Mankoff DA, Dunnwald LK, Partridge SC, Specht JM. Blood flow-metabolism mismatch: good for the tumor, bad for the patient. Clin Canc Res : Off J Am Assoc Canc Res. 2009;15:5294–6. https://doi.org/10.1158/1078-0432.CCR-09-1448.
12. Padhani AR, Miles KA. Multiparametric imaging of tumor response to therapy. Radiology. 2010;256:348–64. https://doi.org/10.1148/radiol.10091760.
13. Shen G, Ma H, Liu B, Ren P, Kuang A. Correlation of the apparent diffusion coefficient and the standardized uptake value in neoplastic lesions: a meta-analysis. Nucl Med Commun. 20176; https://doi.org/10.1097/MNM.0000000000000746.
14. Rakheja R, Chandarana H, DeMello L, Jackson K, Geppert C, Faul D, et al. Correlation between standardized uptake value and apparent diffusion coefficient of neoplastic lesions evaluated with whole-body simultaneous hybrid PET/MRI. AJR Am J Roentgenol. 2013;201:1115–9. https://doi.org/10.2214/AJR.13.11304.
15. Sakane M, Tatsumi M, Kim T, Hori M, Onishi H, Nakamoto A, et al. Correlation between apparent diffusion coefficients on diffusion-weighted MRI and standardized uptake value on FDG-PET/CT in pancreatic adenocarcinoma. Acta Radiol. 2015;56:1034–41. https://doi.org/10.1177/0284185114549825.
16. Chen BB, Tien YW, Chang MC, Cheng MF, Chang YT, Wu CH, et al. PET/MRI in pancreatic and periampullary cancer: correlating diffusion-weighted imaging, MR spectroscopy and glucose metabolic activity with clinical stage and prognosis. Eur J Nucl Med Mol Imaging. 2016;43:1753–64. https://doi.org/10.1007/s00259-016-3356-y.
17. Chen BB, Hsu CY, Yu CW, Liang PC, Hsu C, Hsu CH, et al. Dynamic contrast-enhanced MR imaging of advanced Hepatocellular carcinoma: comparison with the liver parenchyma and correlation with the survival of patients receiving systemic therapy. Radiology. 2016;281:454–64. https://doi.org/10.1148/radiol.2016152659.
18. Tofts PS, Brix G, Buckley DL, Evelhoch JL, Henderson E, Knopp MV, et al. Estimating kinetic parameters from dynamic contrast-enhanced T(1)-weighted MRI of a diffusable tracer: standardized quantities and symbols. J Magnet Res Imaging : JMRI. 1999;10:223–32.
19. Liu K, Xie P, Peng W, Zhou Z. Dynamic contrast-enhanced magnetic resonance imaging for pancreatic ductal adenocarcinoma at 3.0-T magnetic resonance: correlation with histopathology. J Comput Assist Tomography. 2015;39:13–8. https://doi.org/10.1097/RCT.0000000000000171.
20. Wu L, Lv P, Zhang H, Fu C, Yao X, Wang C, et al. Dynamic contrast-enhanced (DCE) MRI assessment of microvascular characteristics in the murine orthotopic pancreatic cancer model. Magn Reson Imaging. 2015;33:737–60. https://doi.org/10.1016/j.mri.2014.08.014.
21. Kim JH, Lee JM, Park JH, Kim SC, Joo I, Han JK, et al. Solid pancreatic lesions: characterization by using timing bolus dynamic contrast-enhanced MR imaging assessment–a preliminary study. Radiology. 2013;266:185–96. https://doi.org/10.1148/radiol.12120111.
22. Yao X, Zeng M, Wang H, Sun F, Rao S, Ji Y. Evaluation of pancreatic cancer by multiple breath-hold dynamic contrast-enhanced magnetic resonance imaging at 3.0T. Europe J Radiol. 2012;81:e917–22. https://doi.org/10.1016/j.ejrad.2012.05.011.
23. Akisik MF, Sandrasegaran K, Bu G, Lin C, Hutchins GD, Chiorean EG. Pancreatic cancer: utility of dynamic contrast-enhanced MR imaging in assessment of antiangiogenic therapy. Radiology. 2010;256:441–9. https://doi.org/10.1148/radiol.10091733.
24. Barral M, Taouli B, Guiu B, Koh DM, Luciani A, Manfredi R, et al. Diffusion-weighted MR imaging of the pancreas: current status and recommendations. Radiology. 2015;274:45–63. https://doi.org/10.1148/radiol.14130778.
25. De Robertis R, Tinazzi Martini P, Demozzi E, Dal Corso F, Bassi C, Pederzoli P, et al. Diffusion-weighted imaging of pancreatic cancer. World J Radiol. 2015;7:319–28. https://doi.org/10.4329/wjr.v7.i10.319.
26. Hecht EM, Liu MZ, Prince MR, Jambawalikar S, Remotti HE, Weisberg SW, et al. Can diffusion-weighted imaging serve as a biomarker of fibrosis in pancreatic adenocarcinoma? J Magnet Res Imaging : JMRI. 2017;46:393–402. https://doi.org/10.1002/jmri.25581.
27. Ma W, Li N, Zhao W, Ren J, Wei M, Yang Y, et al. Apparent diffusion coefficient and dynamic contrast-enhanced magnetic resonance imaging in pancreatic cancer: characteristics and correlation with Histopathologic parameters. J Comput Assist Tomogr. 2016;40:709–16. https://doi.org/10.1097/RCT.0000000000000434.
28. Niwa T, Ueno M, Ohkawa S, Yoshida T, Doiuchi T, Ito K, et al. Advanced pancreatic cancer: the use of the apparent diffusion

coefficient to predict response to chemotherapy. Br J Radiol. 2009;82:28–34. https://doi.org/10.1259/bjr/43911400.

29. Kurosawa J, Tawada K, Mikata R, Ishihara T, Tsuyuguchi T, Saito M, et al. Prognostic relevance of apparent diffusion coefficient obtained by diffusion-weighted MRI in pancreatic cancer. J Magnet Res Imaging : JMRI. 2015; https://doi.org/10.1002/jmri.24939.

30. Penet MF, Shah T, Bharti S, Krishnamachary B, Artemov D, Mironchik Y, et al. Metabolic imaging of pancreatic ductal adeno-carcinoma detects altered choline metabolism. Clin Cancer Res : Off J Am Assoc Canc Res. 2015;21:386–95. https://doi.org/10.1158/1078-0432.CCR-14-0964.

31. Battini S, Faitot F, Imperiale A, Cicek AE, Heimburger C, Averous G, et al. Metabolomics approaches in pancreatic adeno-carcinoma: tumor metabolism profiling predicts clinical outcome of patients. BMC Med. 2017;15:56. https://doi.org/10.1186/s12916-017-0810-z.

32. Nunna P, Sheikhbahaei S, Ahn S, Young B, Subramaniam RM. The role of positron emission tomography/computed tomography in management and prediction of survival in pancreatic cancer. J Comput Assist Tomogr. 2016;40:142–51. https://doi.org/10.1097/RCT.0000000000000323.

33. Chaika NV, Gebregiworgis T, Lewallen ME, Purohit V, Radhakrishnan P, Liu X, et al. MUC1 mucin stabilizes and activates hypoxia-inducible factor 1 alpha to regulate metabolism in pancreatic cancer. Proc Natl Acad Sci U S A. 2012;109:13787–92. https://doi.org/10.1073/pnas.1203339109.

34. Li N, Li Y, Li Z, Huang C, Yang Y, Lang M, et al. Hypoxia inducible factor 1 (HIF-1) recruits macrophage to activate pancreatic Stellate cells in pancreatic Ductal Adenocarcinoma. Int J Mol Sci. 2016;17 https://doi.org/10.3390/ijms17060799.

35. Hoffmann AC, Mori R, Vallbohmer D, Brabender J, Klein E, Drebber U, et al. High expression of HIF1a is a predictor of clinical outcome in patients with pancreatic ductal adenocarcinomas and correlated to PDGFA, VEGF, and bFGF. Neoplasia. 2008;10:674–9.

36. Bali MA, Metens T, Denolin V, Delhaye M, Demetter P, Closset J, et al. Tumoral and nontumoral pancreas: correlation between quantitative dynamic contrast-enhanced MR imaging and histopathologic parameters. Radiology. 2011;261:456–66. https://doi.org/10.1148/radiol.11103515.